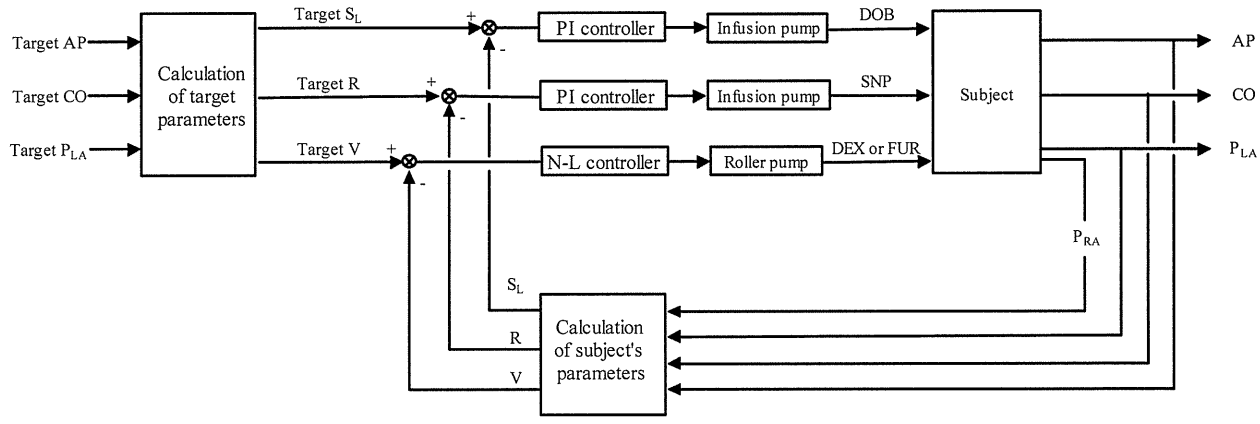

Fig. 2. Schematic illustration of an automated drug delivery system for simultaneous control of AP, CO and P_{LA}. Proportional-integral (PI) feedback controllers adjust infusion rate of DOB and SNP to minimize the difference between target and subject's S_L and those of R, respectively. Nonlinear (N-L) feedback controller adjusts infusion of DEX or injection of FUR to minimize the difference between target and subject's V.

In acute heart failure, cardiac energetic efficiency should also be improved. Theoretically, if heart rate (HR) is reduced while AP, CO and P_{LA} are maintained by preserving S_L with precisely increased LV contractility, it is possible to improve cardiac energetic efficiency and reduce LV oxygen consumption per minute (MVO_2) [8]. In the present study, we also investigated whether this hemodynamics can be accomplished in acute heart failure using our automated drug delivery system.

II. Methods

A. Automated drug delivery system

The integrated CO curve is parameterized by the pumping ability of the left heart (S_L) [ml·min^{-1}·kg^{-1}], the venous return surface by total stressed blood volume (V) [ml·kg^{-1}], and the systemic arterial resistance by R [mmHg·ml^{-1}·min·kg], which are calculated for a given set of AP, CO, P_{LA} and P_{RA} as the following formulas [3];

$$S_L = CO/[\ln(P_{LA} - 2.03) + 0.8] \quad (1)$$

$$V = (CO + 19.61P_{RA} + 3.49P_{LA}) \times 0.129 \quad (2)$$

$$R = (AP - P_{RA})/CO \quad (3)$$

Fig. 2 is a schematic illustration of the automated drug delivery system [3]. Once target values for AP, CO and P_{LA} are defined and fed into the computer, it calculates the target values for S_L, R, and V using Equations (1)-(3). The subject's S_L, R, and V are calculated from measured AP, CO and P_{LA} values using Equations (1)-(3). To minimize the differences between target and subject's S_L and R, proportional-integral feedback controllers adjust the infusion rates of DOB and SNP, respectively. To minimize the difference between target and subject's V, a nonlinear feedback controller adjusts the infusion of DEX or injection of FUR. Gain and rules of the controllers were predefined on the basis of the step responses of S_L, R, and V to the infusions of the drugs [3].

The adjustment processes are repeated in parallel and continued until the differences disappear.

B. Animal experiments to validate performance of the automated drug delivery system

In 12 anesthetized dogs, we acutely created ischemic heart failure by coronary embolization, which decreased CO from 133 ± 42 to 69 ± 22 ml·min^{-1}·kg^{-1}, AP from 109 ± 18 to 91 ± 17 mmHg and increased P_{LA} from 7 ± 2 to 19 ± 6 mmHg.

We connected the animals to the system, and defined target AP (90-105 mmHg), target CO (90-100 ml·min^{-1}·kg^{-1}) and target P_{LA} (8-12 mmHg), which were fed into the system to determine target values for S_L, R, and V as described above. The controllers were then activated by closing the loops. We observed the performance of the system over 50-60 min.

C. Circulatory equilibrium and cardiac energetics

S_L is theoretically related with LV end-systolic elastance (E_{es}, an index of LV contractility), HR, R and diastolic myocardial stiffness (k) as the following formula [7]

$$S_L = \frac{1}{k} \cdot \frac{E_{es}}{(E_{es}/HR) + R} \quad (4)$$

LV Stroke work (SW) is expressed as

$$SW = (AP - P_{LA}) \cdot CO/HR \quad (5)$$

LV pressure-volume area (PVA, an index of total mechanical energy of LV contraction) can be expressed as

$$PVA = AP \cdot AP/2E_{es} + SW \quad (6)$$

LV oxygen consumption per beat (BVO_2) is related to PVA and E_{es} as follows

$$BVO_2 = \alpha \cdot PVA + \beta \cdot E_{es} + \gamma \quad (7)$$

where α, β, and γ are constants. LV mechanical efficiency (ME) and oxygen consumption per minute (MVO_2) are expressed as follows:

$$ME = SW/BVO_2 \quad (8)$$

$$MVO_2 = BVO_2 \cdot HR \quad (9)$$

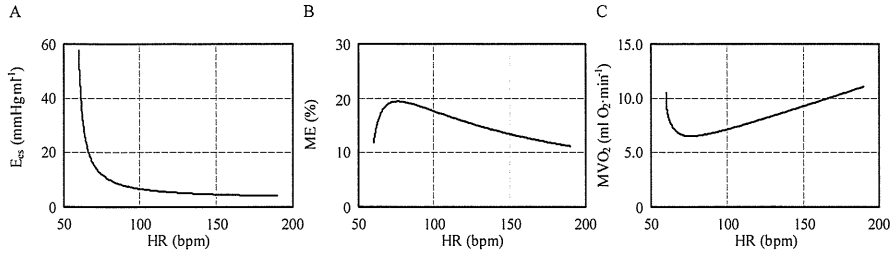

Fig. 3. Simulated relations of heart rate (HR) with left ventricular end-systolic elastance (E_{es}) (**A**), left ventricular mechanical efficiency (ME) (**B**), and left ventricular oxygen consumption per minute (MVO_2) (**C**), when AP, CO and P_{LA} are kept at fixed values.

Using Equations (4)-(9) and fixed values of AP (100 mmHg), CO (100 ml·min^{-1}·kg^{-1}) and P_{LA} (10 mmHg), we numerically simulated the individual relations of HR with E_{es}, ME and MVO_2 (Fig. 3). In these computations, representative k, α, β and γ values (not shown) were used, which are appropriate for a 20-kg dog.

As indicated in Fig. 3, HR is inversely related to E_{es} (Fig. 3A). Over the physiological range of HR for dogs (>80 bpm), ME increases as HR is reduced (Fig. 3B), i.e. cardiac energetic efficiency is optimized. At HR of 75 bpm, ME becomes maximal and MVO_2 becomes minimal (Fig. 3B, C). When HR is reduced from 150 to 110 bpm, E_{es} increases from 4.6 to 5.9 mmHg·ml^{-1} (29% increase) and ME increases from 13 % to 17 % (24 % increase), whereas MVO_2 decreases from 8.9 to 7.2 ml O_2·min^{-1} (19% reduction) [8]. This indicates that as long as HR is within the physiological range, HR reduction together with compensatory LV inotropy (an increase of E_{es}) consistently improves cardiac energetic efficiency and reduces MVO_2.

D. Animal experiments to optimize cardiac energetics using the automated drug delivery system

In 7 anesthetized dogs, we acutely created ischemic heart failure by coronary embolization, which decreased CO from 101±5 to 62±13 ml·min^{-1}·kg^{-1}, AP from 114±4 to 97±14 mmHg and increased P_{LA} from 9 ± 1 to 17±2 mmHg. Zatebradine (0.5 mg·kg^{-1}) was administered intravenously to suppress the intrinsic atrial beat, and atrial pacing was then initiated to control HR (146±8 bpm). After induction of acute heart failure, cardiac energetics were evaluated (*AHF*).

We activated the system with target values of 90-100 mmHg for AP, 80-100 ml/kg/min for CO and 10-12 mmHg for P_{LA}. The system restored AP, CO and P_{LA} to their respective target values within 30 min. After confirming stable hemodynamics, cardiac energetics were evaluated (*Initial HR*). We then reduced the pacing rate in steps of 10 or 20 bpm. The maximum HR reduction (*Lowest HR*) averaged 39±12 bpm. For each HR step, we waited for hemodynamic stabilization, and the measurements of cardiac energetics were performed.

III. Results

A. Performance of the automated drug delivery system

Fig. 4 shows the experimental trial in a representative animal. The system was activated at 0 min. Fig. 4A shows the time courses of the infusion rates of DOB and SNP, and the accumulated volume of infused DEX. In this case, FUR was not injected. Fig. 4B shows the time courses of S_L, R and V. Infusion rates of DOB, SNP, and DEX were adjusted so that S_L, R and V reached their respective target values. By controlling the cardiovascular parameters, the automated system controlled AP, CO and P_{LA} accurately and stably as demonstrated in Fig. 4C. AP, CO and P_{LA} reached their respective target levels within 30 min and remained at these levels.

In 12 animals, the average times for AP, CO and P_{LA} to reach the acceptable ranges (± 10 mmHg of target AP, ± 10 ml·min^{-1}·kg^{-1} of target CO, ± 2 mmHg of target P_{LA}) were 5.2 ± 6.6 min, 6.8 ± 4.6min, and 11.7 ± 9.8 min, respectively. The average standard deviations from the target values were small for AP [4.4 ± 2.6mmHg], CO [5.4 ± 2.4ml·min^{-1}·kg^{-1}] and P_{LA} [0.8 ± 0.6 mmHg].

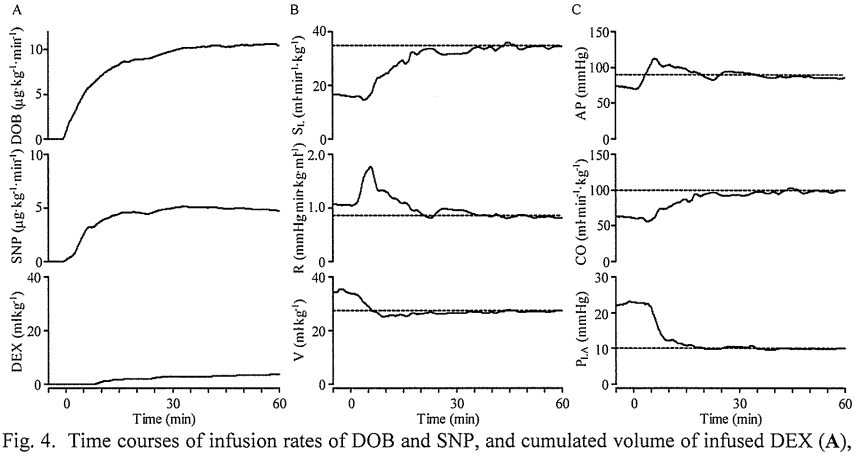

Fig. 4. Time courses of infusion rates of DOB and SNP, and cumulated volume of infused DEX (**A**), cardiovascular parameters (**B**), and hemodynamic variables (**C**) in one representative animal during closed-loop control of hemodynamics. Broken horizontal lines in panel B and C indicate target values.

B. Cardiac energetics improved following bradycardia while preserving normal hemodynamics in heart failure

In seven anesthetized dogs with acute heart failure, the automated drug delivery system restored and maintained normal hemodynamics (CO; 88±3 ml·min^{-1}·kg^{-1}, P_{LA};

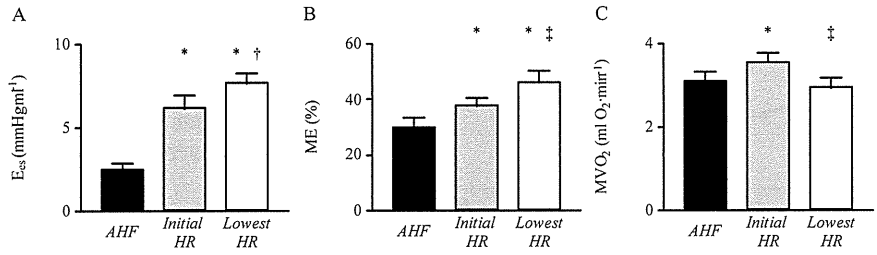

Fig. 5. Cardiac energetics after coronary artery embolization (*AHF*), at the initial HR (*Initial HR*), and at the lowest HR (*Lowest HR*). E_{es}, left ventricular (LV) end-systolic elastance; ME, LV mechanical efficiency; MVO_2, LV oxygen consumption per minute. Data are means ± SEM. *: $P<0.01$ vs *AHF*. †: $P<0.05$, ‡: $P<0.01$ versus *Initial HR*.

10.9±0.4 mmHg), even when zatebradine significantly reduced HR (107±7 bpm, -27±3%).

Fig. 5 summarizes cardiac energetics at *AHF*, *Initial HR*, and *Lowest HR*. When the data at *Initial HR* and *Lowest HR* were compared with those at *AHF*, E_{es} and ME increased significantly. MVO_2 at *Initial HR* also increased compared to that at *AHF*, although MVO_2 at *Lowest HR* was almost identical to that at *AHF*. The automated drug delivery system restored normal hemodynamics with increased energy cost at *Initial HR*, but with diminished energy cost at *Lowest HR*. Comparing the data at *Lowest HR* with those at *Initial HR*, E_{es} increased (+34±14 %), ME increased (+22±6 %) and MVO_2 decreased significantly (-17±4 %). Changes in the LV mechanoenergetic data following HR reduction averaged over seven animals are compatible with those predicted theoretically (Fig. 3).

IV. Discussion

A. Characteristics of our system

Our system controls the mechanical determinants of circulation, and as a result achieves target values for hemodynamic variables [3]. Previous systems attempted to control hemodynamic variables by estimating the apparent input–output relations between drug infusion and response of the controlled variables. In the systems that control AP and CO, all possible input–output relations have to be estimated; namely, inotrope–AP, inotrope–CO, vasodilator–AP, and vasodilator–CO relations [2]. The reason is that these drugs affect AP and CO simultaneously to almost the same degree. If this previous approach is applied to simultaneous control of AP, CO and P_{LA}, at least 9 input–output relations have to be estimated, since at least 3 drugs are required to independently control the three variables. This would make the system extremely complicated, and therefore be practically unfeasible. The three drug controllers in our system (Fig. 2) are designed on the basis of only three input–output relations between drug infusion and response of the controlled parameter; namely, DOB–S_L, SNP–R and DEX/FUR–V. The fact that the three closed loops are effectively decoupled simplifies the entire system. This also permits a system operator, who would be a physician untrained in control engineering, to understand its behavior easily

B. Simultaneous optimization of cardiac energetic and hemodynamics

The degree of reduction in MVO_2 (17 %, *Lowest HR* vs *Initial HR* in Fig. 5C) when HR was reduced by 30% in the present experiment is less than that observed in beta-blockade treatment. For example, atenolol decreased MVO_2 by 40% when HR was reduced by 30% in dogs during exercise. Negative ventricular inotropy accompanying HR reduction accounts for the further reduction in MVO_2 achieved by beta-blockade. However, in acute heart failure, use of beta-blockers is contraindicated owing to its adverse effects on systemic hemodynamics. Taken together, the degree of reduction in MVO_2 obtained in this study is reasonable considering that it is achieved without sacrificing the normal hemodynamic condition.

V. Conclusion

By directly controlling the mechanical properties of the heart and vessel, our automated system enables comprehensive management of hemodynamics in acute heart failure.

References

[1] W. R. Chitwood Jr., D. M. Cosgrove 3rd., R. M. Lust, "Multicenter trial of automated nitroprusside infusion for postoperative hypertension. Titrator Multicenter Study Group," *Ann. Thorac. Surg.* vol. 54, no. 3, 517-522, Sep. 1992.

[2] C. Yu, R. J. Roy, H. Kaufman, B. W. Bequette, "Multiple-model a daptive predictive control of mean arterial pressure and cardiac output," *IEEE. Trans. Biomed. Eng.* vol. 39:765-778, 1992.

[3] K. Uemura, A. Kamiya, I. Hidaka, T. Kawada, S. Shimizu, *et al.*, "Automated drug delivery system to control systemic arterial pressure, cardiac output, and left heart filling pressure in acute decompensated heart failure," *J. Appl. Physiol.* vol. 100, no 4, 1278-1286, Apr. 2006.

[4] A. C. Guyton, "Determination of cardiac output by equating venous return curves with cardiac response curves," *Physiol. Rev.* vol. 35, no. 1,123–129, Jan. 1955.

[5] K. Sunagawa, K. Sagawa, W. L. Maughan, "Ventricular interaction with the loading system," *Ann. Biomed. Eng.* vol. 12, no. 2, 163-189, 1984.

[6] K. Uemura, M. Sugimachi, T. Kawada, A. Kamiya, Y. Jin, *et al.*, "A novel framework of circulatory equilibrium," *Am. J. Physiol. Heart Circ. Physiol.* vol. 286, no. 6, pp. H2376–H2385, Jun. 2004.

[7] K. Uemura, T. Kawada, A. Kamiya, T. Aiba, I. Hidaka, *et al.*, "Prediction of circulatory equilibrium in response to changes in stressed blood volume," *Am. J. Physiol. Heart Circ. Physiol.* vol. 289, no. 1, H301–H307, Jul. 2005.

[8] K. Uemura, K. Sunagawa, M. Sugimachi, "Computationally managed bradycardia improved cardiac energetics while restoring normal hemodynamics in heart failure," *Ann. Biomed. Eng.* vol. 37, no. 1, 82-93, Jan. 2009.

32nd Annual International Conference of the IEEE EMBS
Buenos Aires, Argentina, August 31 - September 4, 2010

Estimated Venous Return Surface and Cardiac Output Curve Precisely Predicts New Hemodynamics after Volume Change

Masaru Sugimachi, *Member, IEEE*, Kenji Sunagawa, *Member, IEEE*,
Kazunori Uemura, Atsunori Kamiya, Shuji Shimizu, Masashi Inagaki and Toshiaki Shishido

Abstract— **In our extended Guyton's model, the ability of heart to pump blood is characterized by a cardiac output curve and the ability of vasculature to pool blood by a venous return surface. These intersect in a three-dimensional coordinate system at the operating right atrial pressure, left atrial pressure, and cardiac output. The baseline cardiac output curve and venous return surface and their changes after volume change would predict new hemodynamics. The invasive methods needed to precisely characterize cardiac output curve and venous return surface led us to aim at estimating cardiac output curve and venous return surface from a single hemodynamic measurement. Using the average values for two logarithmic function parameters, and for two slopes of a surface, we were able to estimate cardiac output curve and venous return surface. The estimated curve and surface predicted new hemodynamics after volume change precisely.**

I. Introduction

OUR group has developed an extended Guyton's cardiovascular model, where the ability of the right- and left-sided heart to pump blood is integratively characterized by a single curve (cardiac output curve) and the ability of vasculature to pool blood is expressed as a surface (venous return surface). The cardiac output curve and the venous return surface intersect in a three-dimensional coordinate system, and the three coordinates show the operating right atrial pressure (RAP), left atrial pressure (LAP), and cardiac output (CO), respectively (Fig. 1).

If one knows the baseline cardiac output curve and venous return surface and how these change after volume infusion and depletion, one can predict new hemodynamics by combining a new cardiac output curve and a new venous return surface. The precise characterization of cardiac output curve and venous return surface, however, needs extremely invasive measures for changing loading conditions to be applicable to patients with heart diseases (see Sections IIB and IIC for the detailed invasive methods used in animal experiments). Therefore, the aim of this study was to circumvent this difficulty by establishing a method to approximately obtain the cardiac output curve and venous return surface from a single hemodynamic measurement.

Manuscript received April 7, 2009. This work was supported in part by Grant-in-Aid for Scientific Research (B 20300164, C 20500404) from the Ministry of Education, Culture, Sports, Science and Technology, by Health and Labour Sciences Research Grants (H20-katsudo-shitei-007) from the Ministry of Health Labour and Welfare of Japan.

M. Sugimachi, K. Uemura, A. Kamiya, S. Shimizu, M. Inagaki and T. Shishido are with the National Cardiovascular Center Research Institute, Suita, Osaka 5658565, Japan (corresponding author Masaru Sugimachi to provide phone: +81-6-6833-5012; fax: +81-6-6835-5403; e-mail: su91mach@ri.ncvc.go.jp).

K. Sunagawa is with Kyushu University, Fukuoka 8128582 Japan. (e-mail: sunagawa@cardiol.med.kyushu-u.ac.jp).

II. Model and Methods

A. Extended Guyton's Model

We have extended Guyton's model [1] to handle a number of difficulties frequently encountered in clinical settings in patients with predominantly unilateral heart failure.

First, we extended a 2D (RAP-CO) Guyton's model to a 3D (RAP-LAP-CO) model, and introduced a third axis for LAP (Fig. 1) [2], [3]. By this modification, we can get the operating LAP directly from the intersection between cardiac output curve and venous return surface. LAP indicates the degree of pulmonary congestion and inadequate blood oxygenation, and normal range of LAP is as important as that of cardiac output and that of blood pressure for sustaining life.

Second, in this 3D model, we can separately express the changes in pumping ability of the right- and left-sided heart; the 3D cardiac output curve (Fig. 1, thick curve) is, in reality, the integration of two separate 2D cardiac output curves. The pumping ability of the right-sided heart can be obtained by projecting the 3D curve to the RAP-CO plane, and that of the

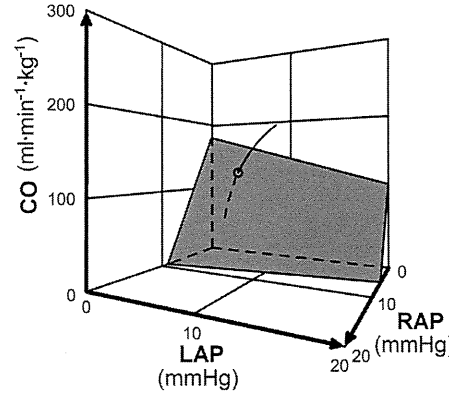

Fig. 1. An extended Guyton's model. The curve integratively expresses the pumping ability of right- and left-sided heart. The shaded surface characterizes the blood-pooling ability of the vasculature. RAP, right atrial pressure; LAP, left atrial pressure; CO, cardiac output (per kg of body weight).

left-sided heart can be obtained by projecting it to the LAP-CO plane. The preferential decrease in the pumping ability of the left-sided heart, such as seen in the ischemic heart disease, would rotate the projected curve to the RAP-LAP plane to the direction of LAP axis.

Third, the blood-pooling ability of the vasculature and the effect of stressed blood on the vasculature can be expressed by the venous return surface (Fig. 1, shaded surface). This surface remains the same so long as the total stressed volume is unchanged irrespective of its distribution. Increased LAP and pulmonary congestion associated with left-sided heart failure is characterized by blood redistribution from systemic to pulmonary vascular beds. Blood redistribution, however, would not change the venous return surface itself (i.e., unaffected by the changes in pumping ability). This is in sharp contrast with the classical venous return curve of Guyton's model. The relatively flat slope of the surface to the direction of LAP axis indicates the smaller blood-pooling ability of pulmonary vascular beds. As a result, the decrease in RAP with systemic-to-pulmonary blood redistribution is much smaller than the increase in LAP. This is shown, also illustratively in Fig. 1, by moving along the venous return surface and parallel to the RAP-LAP plane (keeping CO constant).

B. Animal Experiments to Characterize Cardiac Output Curve

We planned to characterize both cardiac output curve and venous return surface as precisely as possible in animals by using even the most invasive methods. In characterizing the pumping ability, only the heart of animals is needed; in characterizing the blood-pooling ability, only the vasculature of animals is needed.

The experiment for the characterization of cardiac output curve was less invasive. We do not need to physically detach the vasculature from the heart. Rather, in 7 dogs, by withdrawing and transfusing blood in a stepwise manner, we were able to obtain both right- and left-sided cardiac output curve simultaneously.

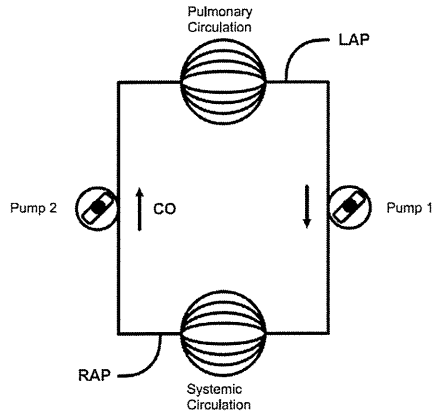

Fig. 2. An experimental scheme to characterize venous return surface. By replacing the right- and the left-sided heart with respective roller pumps, one can change cardiac output of the right- and the left-sided heart independently.

C. Animal Experiments to Characterize Venous Return Surface

Figure 2 depicts the scheme of an experiment to characterize the venous return surface. To extract only the vasculature and to physically remove the animal heart from the cardiovascular system, we replaced the right- and the left-sided heart with respective roller pumps. These pumps allow us to change CO of the right- and left-sided heart independently. Changing the flow of the two pumps at the same level would simulate the weak or strong heart. Transient unbalancing flow would redistribute blood between systemic and pulmonary vascular beds.

In each of 6 canine preparations, we obtained 6 different hemodynamic (CO, RAP, LAP) data sets. In each animal, these sets of data were fit to a flat surface in 3D coordinate system by linear regression analysis. CO was selected as a dependent variable and RAP (~2-5 mmHg) and LAP (~0-10 mmHg) are selected as independent variables.

D. Method to Estimate Cardiac Output Curve from a Single Hemodynamic Data Set

We fit experimental data to two logarithmic curves (one for the right- and the other for the left-sided heart), based on the knowledge of exponential end-diastolic pressure volume relationship and linear end-systolic pressure volume relationship, as follows.

$$CO = S\,[\ln(P - A) + B]$$

Here, P indicates RAP or LAP; A, B, and S are parameters. As analytical solution indicated that A and B is only dependent on diastolic properties of the ventricles, and is unlikely to change acutely, we fixed these parameters as their respective average values. This enabled one to estimate cardiac output curve from a single hemodynamic data set.

E. Method to Estimate Venous Return Surface from a Single Hemodynamic Data Set

We were able to fit experimental data to a flat surface well (r^2=0.92 to 0.99). As the surfaces from 6 animals were reasonably parallel (see Results), we used average slopes to estimate venous return surface from a single hemodynamic data set. Furthermore, as CO-axis intercept was linearly related to the withdrawn or transfused blood volume, we used this relationship to estimate a new venous return surface after blood volume change.

III. Results

A. Method to Estimate Cardiac Output Curve from a Single Hemodynamic Data Set

We were able to fit the cardiac output curve of both the right- and the left-sided heart by logarithmic functions (right-sided heart, r^2=0.90 to 0.99; left-sided heart, r^2=0.95 to 0.99). Since standard deviation of parameter A (1.29) or that of parameter

B (1.25) was much smaller than that of parameter S (30.9), we used the respective average values for A and B. The obtained cardiac output curves for right- and left-sided heart were as follows.

$$CO = S_R [\ln(RAP - 2.13) + 1.90] \quad (1)$$

$$CO = S_L [\ln(LAP - 2.03) + 0.80] \quad (2)$$

Parameters S_R and S_L can be used to represent the magnitude of the pumping ability of the right- and left-sided heart, respectively. As S_R and S_L can be calculated from a single set of hemodynamic data, we can approximately get cardiac output curve.

B. Method to Estimate Cardiac Output Curve from a Single Hemodynamic Data Set

In Figure 3 we have shown the venous return surfaces obtained from all 6 dogs. The surfaces were shown (as if they were lines) from the direction parallel to the surface. The figure indicates that in each of 6 dogs, all 6 data sets are located very near the flat surface. This implied the goodness of the fit of these data points to the flat surface. It is also shown that three coordinate axes are almost parallel among these dogs. This is because the slopes of the surface were almost the same among animals. These experimental results indicated that the venous return surface is linear and can be expressed by a common equation for all animals.

$$CO = CO_{max} - 19.61\ RAP - 3.49\ LAP.$$

Further, by infusing or withdrawing known amounts of blood, we were able to relate CO_{max} to blood volume as

$$CO_{max} = V / 0.129 \quad (3)$$

where V is total intravascular stressed blood volume. Combining these equations resulted in

$$CO = V / 0.129 - 19.61\ RAP - 3.49\ LAP. \quad (4)$$

Parameter V can be used to monitor the changes in total stressed blood volume. As V can be calculated from a single set of hemodynamic data, we can approximately get venous return surface.

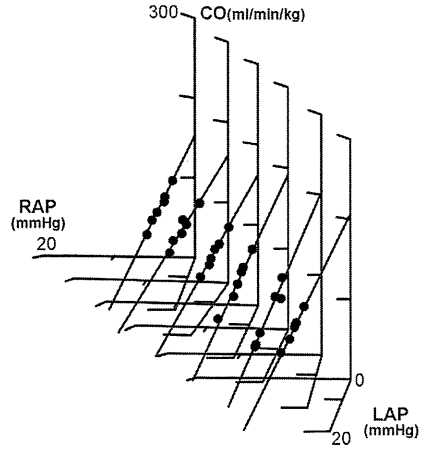

Fig. 3. Venous return surfaces obtained from 6 dogs. For each dog, the venous return surface was projected in a direction parallel to the surface, and was superimposed with each other.

C. Prediction of New Hemodynamics after Volume Change

We predicted new hemodynamics after volume change as follows. First, baseline cardiac output curve (Equations 1 and 2) and venous return surface (Equation 4) were approximately estimated from a single baseline hemodynamic data, by the methods shown in two previous sections IIIA and IIIB. Next, a new venous return surface was estimated by changing CO_{max} according to Equation 3. We assumed that cardiac output curve would not change by the volume change. Finally, new hemodynamics data were estimated by calculating the intersection between cardiac output curve and venous return surface.

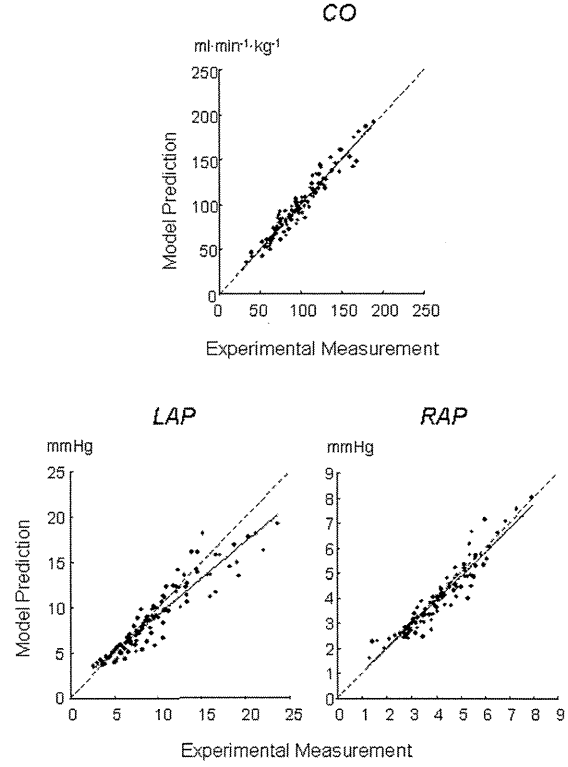

Fig. 4. Prediction of CO, LAP, and RAP from estimated cardiac output curve and venous return surface after volume change.

Using these new estimated cardiac output curve and venous return surface, we were able to predict the hemodynamics (y value) after withdrawal or transfusion of blood of known volume precisely as compared to actually measured (x value) (CO: $y = 0.93x + 6.5$, $r^2 = 0.96$, SEE [standard error of estimate] = 7.5 $ml \cdot min^{-1} \cdot kg^{-1}$; LAP: $y = 0.90x + 0.5$, $r^2 = 0.93$, SEE = 1.4 mmHg; RAP: $y = 0.87x + 0.4$, $r^2 = 0.91$, SEE = 0.4 mmHg) (Fig. 4) [3].

IV. Discussion

A. Most Undiagnosed Property: Total Stressed Blood Volume

The three major players of the cardiovascular system are heart

(pumps), vasculature (tubes with resistive and capacitive function), and blood. These three components interactively determine all hemodynamic variables. Of these, pump function and resistive function of vasculature have been repeatedly evaluated in previous studies. These properties were also evaluated clinically.

In contrast, evaluation of the vascular capacitive function and that of the blood volume have been relatively ignored. Even though blood volume drastically changes, there have been no reasonable methods to evaluate total stressed blood volume precisely. Simple measurement of central venous pressure (i.e., RAP) cannot be a proxy marker of blood volume, as this pressure value also changes with pump function or with redistribution of blood.

It is clear from our results [V = (CO + 19.61 RAP + 3.49 LAP) × 0.129] that blood volume (V) is not solely determined by RAP. Rather, all three variables CO, RAP and LAP contribute (not as differently as have been considered) to the changes in blood volume. Clinicians should know that when LAP increases by 5.6 mmHg, or CO increases by 0.98L/min in 50-Kg patients, similar blood volume increases as RAP is increased by 1 mmHg.

Implantable devices with volume monitoring functionality for patients with heart failure should also take these results into consideration.

B. Hemodynamic Variables and Cardiovascular Properties

In clinical practice, physicians have to restore hemodynamic variables to their respective normal range. Of these, the most important three variables include blood pressure, CO and LAP. These variables are essentially important as blood pressure determines the perfusion of vital organs (for short-term need), CO determines the perfusion of peripheral tissues (for long-term need), and LAP determines blood oxygenation in lungs.

These hemodynamic variables are, in turn, determined by the interaction between cardiovascular properties, such as pump, resistance, capacitance, and blood volume. What clinicians should know, monitor, and correct are in reality these cardiovascular properties. Most drugs and interventions are aimed at correcting mainly one of these properties. From these viewpoints, the method to continuously estimate cardiovascular properties from measured hemodynamics is the most basic need in patient monitoring.

V. Conclusion

We have successfully developed a method to estimate the cardiac output curve and venous return surface from a single hemodynamic data set. This method enabled to predict new hemodynamics after withdrawal or transfusion of blood of known volume.

References

[1] A. C. Guyton, "Determination of cardiac output by equating venous return curves with cardiac response curves," *Physiol. Rev.* vol. 35, no. 1,123–129, Jan. 1955.

[2] K. Uemura, M. Sugimachi, T. Kawada, A. Kamiya, Y. Jin, *et al.*, "A novel framework of circulatory equilibrium," *Am. J. Physiol. Heart Circ. Physiol.* vol. 286, no. 6, pp. H2376–H2385, Jun. 2004.

[3] K. Uemura, T. Kawada, A. Kamiya, T. Aiba, I. Hidaka, *et al.*, "Prediction of circulatory equilibrium in response to changes in stressed blood volume," *Am. J. Physiol. Heart Circ. Physiol.* vol. 289, no. 1, H301–H307, Jul. 2005.

32nd Annual International Conference of the IEEE EMBS
Buenos Aires, Argentina, August 31 - September 4, 2010

How to quantitatively synthesize dynamic changes in arterial pressure from baroreflexly modulated ventricular and arterial properties

Takafumi Sakamoto, Yoshinori Murayama, Tomoyuki Tobushi, Kazuo Sakamoto, Atsushi Tanaka, Takaki Tsutsumi, and Kenji Sunagawa, Senior *Member, IEEE*

Abstract—**Baroreflex regulates arterial pressure by modulating ventricular and vascular properties. We investigated if the framework of circulatory equilibrium that we developed previously (Am J Physiol 2004, 2005) by extending the classic Guyton's framework is capable of predicting baroreflex induced changes in arterial pressure. In animal experiments, we estimated open loop transfer functions of baroreflexly modulated ventricular and vascular properties, synthesized baroreflex induced dynamic changes in arterial pressure using the estimated transfer functions and compared the predicted responses with measured responses. We demonstrated that the predicted baroreflex induced changes in arterial pressure matched reasonable well with those measured. We conclude that the framework of circulatory equilibrium is generalizable under the condition where baroreflex dynamically changes arterial pressure.**

I. Introduction

Baroreflex is known to be the fastest mechanism in the body to stabilize arterial pressure (AP). This AP stabilization is achieved by feedback regulation of ventricular and vascular properties [1-3]. However, how those changes in mechanical properties quantitatively impact AP remains unknown. We previously developed a framework of circulatory equilibrium where we introduced the left atrial pressure-cardiac output (CO) relationship into the classic Guyton's framework and expanded the venous return (VR) curve to the VR surface. We then expressed the CO curves and VR surface using end-systolic elastance (Ees), heart rate (HR), vascular resistance (R) and stressed blood volume (V) [4, 5] and derived the circulatory equilibrium as the intersection between the CO curve and VR surface. The purpose of this investigation is if the extended Guyton's framework can quantitatively predict dynamic AP responses by incorporating the baroreflexly modulated ventricular and arterial properties.

Manuscript received April 23, 2010. This work was supported in part by Health and Labour Sciences Research Grant for Research on Medical Devices for Improving Impaired QOL from the Ministry of Health Labour and Welfare of Japan, Health and Lobour Sciences Research Grant for Clinical Research from the Ministry of Health Labour and Welfare of Japan, and Grant-in-Aid for Scientific Research(S) (18100006) from the Japan Society for the Promotion of Science

T. Sakamoto, Y. Murayama, T. Tobushi, K. Sakamoto, A. Tanaka and K. Sunagawa are with Kyushu university, Fukuoka 8128582 Japan. (corresponding author Takafumi Sakamoto to provide phone: +81-92-642-5360; fax: +81-92-642-5357; e-mail: tsaka@cardiol.med.kyushu-u.ac.jp).

T. Tsutsumi is with Iizuka Hospital, Iizuka 8208505 Japan (e-mail: tsutsumi@cardiol.med.kyushu-u.ac.jp).

II. Methods

A. A framework of circulatory equilibrium

The framework of circulatory equilibrium consists of the VR surface representing VR of the systemic and pulmonary circulations and the integrated CO curve representing the pumping ability of the left (LV) and right ventricle (RV) (Fig. 1) [4, 5]. The integrated CO curve and VR surface (CO*v*) are formulated as

$$CO = \frac{1}{k} \times \frac{Ees}{Ees/HR + R} \times \{\log(Pat - F) + H\}$$

and

$$COv = V/w - Gp \times P_{LA} - Gs \times P_{RA}$$

respectively, where Pat is left atrial pressure (P_{LA}) for LV and right atrial pressure (P_{RA}) for RV. k, F, H, w, Gp and Gs are empirically derived constants. Once we obtain a set of Ees, R, HR and V, we derive CO by the framework and estimate AP by multiplying CO and R [4, 5].

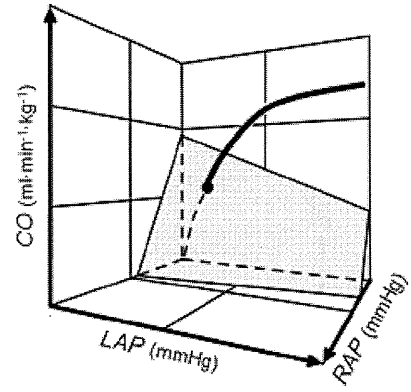

FIG.1 A FRAMEWORK OF CIRCULATORY EQUILIBRIUM

B. Animal preparation

Animal care was in accordance with institutional guidelines. Six mongrel dogs weighing 16.5±1.2kg (mean±SD) were anesthetized with pentobarbital sodium. We cut the vagosympathetic trunk to eliminate other reflexes and isolated

the bilateral carotid sinuses from the systemic circulation and connected them to a servo pump to control intrasinus pressure (CSP). An ultrasonic flow probe was placed around the ascending aorta to measure CO. We implanted two pairs of sonomicrometer in the epicardium and inserted a micromanometer into LV via the apex to measure Ees. We measured AP, P_{LA} and P_{RA}. Stressed blood volume was estimated from the VR surface. All analog data were digitalized at 200Hz with 12-bit resolution.

C. *Identification of the transfer function*

We perturbed CSP with pseudorandom binary sequences (100 and 180 mmHg) with a shortest interval of 5 seconds to identify the open-loop transfer functions from CSP to Ees, HR, R and V. We estimated the transfer functions in the frequency range between 0.002 to 0.1 Hz. To quantify the linear dependence between the input and output signals in the frequency domain, we also estimated a magnitude-squared coherence function.

D. *Prediction of the dynamic change of AP*

To validate the framework of circulatory equilibrium, we predicted Ees, HR, R and V using those estimated transfer functions in response to changes in CSP in data sets that had not been used to estimate the transfer functions. We then predicted APs using the developed framework and compared them against measured.

III. RESULTS

Mean AP, HR, Ees, R and V during perturbations were 124±22 mmHg, 168±13 bpm, 11.3±2.9 mmHg/ml, 1.37±0.27 ml/(ml/min/kg) and 18.8±3.7 ml/kg, respectively. These values are comparable to those previously reported [4, 5].

Shown in Fig. 2 is the transfer function from CSP to Ees in an animal. The transfer function approximates a second-order delay system with a cut-off frequency of 0.023 Hz. These finding are consistent with that reported [2].

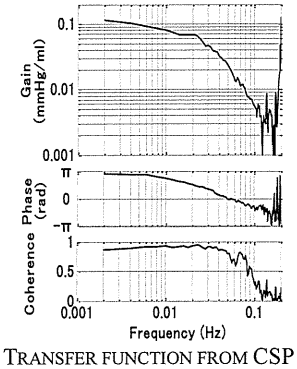

FIG. 2. TRANSFER FUNCTION FROM CSP TO Ees

Illustrated in Fig. 3 are the time series of CSP, predicted AP (solid line) and measured AP (dotted line) in an animal. The predicted AP matches reasonably well with those measred. The correlation coefficent (r2) varied between 0.80 and 0.93. The standard error of estimate ranged between 4.4 and 7.6 mmHg (3.0-7.2 % of mean AP) suggseting the reasonable accuracy of prediction.

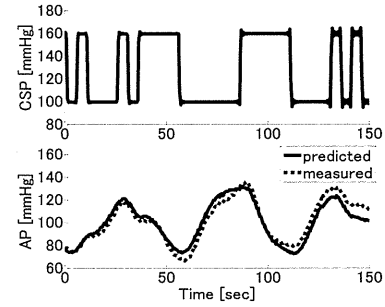

FIG. 3. PREDICTION OF THE DYNAMIC CHANGE OF AP

IV. DISCUSSION

We have shown that the framework of circulatory equilibrium, which is an extension of the classic Guyton's framework, could predict the changes of AP induced by baroreflexly modulated ventricular and vascular properties.

The extended Guyton's framework developed by the authors' group has been shown to accurately represent the circulatory equilibrium under steady state conditions [4, 5]. However, whether the model holds under dynamic conditions remained unanswered. Furthermore, in the present study, we predicted the dynamic baroreflex induced responses of Ees, HR, R and V with a set of linear transfer functions. Since the baroreflex system is known to be nonlinear, how the nonlinearity in the baroreflex system impacts the accuracy of predictions remained unknown. The results of present study indicated that we could linearly predict baroreflexly modulated ventricular and vascular properties reasonably well and the framework of circulatory equilibrium holds under the condition where baroreflex dynamically changes arterial pressure.

V. CONCLUSION

We conclude that the proposed framework of circulatory equilibrium holds under baroreflex induced dynamic changes in hemodynamic conditions.

ACKNOWLEDGMENT

This study was supported in part by Health and Labour Sciences Research Grant for Research on Medical Devices for Improving Impaired QOL from the Ministry of Health Labour and Welfare of Japan, Health and Labour Sciences Research Grant for Clinical Research from the Ministry of Health Labour and Welfare of Japan, and Grant-in-Aid for Scientific Research(S) (18100006) from the Japan Society for the Promotion of Science.

REFERENCES

[1] A.C. Guyton, and John E. Hall, "Textbook of Medical Physiology, eleventh edition", *pp. 230-231. 2006.*

[2] T. Kubota, J. A. Alexander Jr, R. Itaya, K. Todaka, M. Sugimachi, K. Sunagawa, Y. Nose and A. Takeshita, "Dynamic effects of carotid

sinus baroreflex on ventriculoarterial coupling studied in anesthetized dogs,'' *Circulation Research ; 70: 1044-1053, 1992.*

[3] A. A. Shoukas, ''Carotid sinus baroreceptor reflex control and epinephrine. Influence on capacitive and resistive properties of the total pulmonary vascular bed of the dog,'' *Circulation Research ; 51; 95-101, 1982*

[4] K. Uemura, M. Sugimachi, T. Kawada, A. Kamiya, Y. Jin, K. Kashihara, and K. Sunagawa, "A novel framework of circulatory equilibrium,'' *Am J Physiol Heart Circ Physiol 286: H2376-H2385, 2004.*

[5] K. Uemura, T. Kawada, A. Kamiya, T. Aiba, I. Hidaka, K. Sunagawa, and M. Sugimachi, "Prediction of circulatory equilibrium in response to changes in stressed blood volume,'' *Am J Physiol Heart Circ Physiol 289: H301-H307, 2005.*

Atherosclerosis 213 (2010) 52–58

Contents lists available at ScienceDirect

Atherosclerosis

journal homepage: www.elsevier.com/locate/atherosclerosis

Acetylcholinesterase inhibitors attenuate atherogenesis in apolipoprotein E-knockout mice

Keita Inanaga[a], Toshihiro Ichiki[a,b,*], Ryohei Miyazaki[a], Kotaro Takeda[a,b], Toru Hashimoto[a], Hirohide Matsuura[a], Kenji Sunagawa[a]

[a] Department of Cardiovascular Medicine, Kyushu University Graduate School of Medical Sciences, Japan
[b] Department of Advanced Therapeutics for Cardiovascular Diseases, Kyushu University Graduate School of Medical Sciences, Japan

ARTICLE INFO

Article history:
Received 16 February 2010
Received in revised form 7 July 2010
Accepted 18 July 2010
Available online 27 July 2010

Keywords:
Cholinesterase inhibitor
Donepezil
Apolipoprotein E-knockout mice
Oxidative stress
Cytokine

ABSTRACT

Objective: Donepezil, a reversible acetylcholinesterase inhibitor, improves cognitive function of Alzheimer's disease. Stimulation of cholinergic system was reported to improve long-term survival of rats with chronic heart failure and to attenuate inflammatory response in mice with lipopolysaccharide-induced sepsis. We sought to determine whether the pharmacological stimulation of cholinergic system by donepezil reduces atherogenesis in apolipoprotein (Apo) E-knockout (KO) mice.

Methods and results: Male ApoE-KO mice (10-week-old) were fed a high-fat diet and received infusion of angiotensin (Ang) II (490 ng/kg/day). Donepezil or physostigmine was administered for 4 weeks. Oral administration of donepezil (5 mg/kg/day) or infusion of physostigmine (2 mg/kg/day) significantly attenuated atherogenesis (Oil Red O-positive area) without significant changes in heart rate, blood pressure and total cholesterol levels. Administration of donepezil suppressed expression of monocyte chemoattractant protein-1 and tumor necrosis factor-α, NADPH oxidase activity and production of reactive oxygen species in the aorta.

Conclusion: The present study revealed novel anti-oxidative and anti-atherosclerotic effects of pharmacological stimulation of cholinergic system by donepezil. Donepezil may be used as a novel therapeutics for the atherosclerotic cardiovascular diseases.

1. Introduction

Activation of vagus nerve shows various effects on hemodynamics. It slows heart rate, dilates blood vessel and reduces blood pressure. Results of the Autonomic Tone and Reflexes After Myocardial Infarction Study and the Cardiac Insufficiency Bisoprolol Study II indicate that diminished cardiac vagus activity predicts the higher mortality rate in patients with chronic heart failure [1,2]. In addition, vagus nerve stimulation (VNS) improves long-term survival of rats with chronic heart failure after experimental myocardial infarction [3]. VNS modulates the cardiac redox status and adrenergic drive, and thereby suppresses free radical generation in the failing heart [4]. However, the effect of VNS on vascular lesion formation has not been reported.

Stimulation of cholinergic system was reported to attenuate tumor necrosis factor (TNF)-α production from macrophages and hypotensive shock in a lipopolysaccharide (LPS)-induced septic model [5,6]. Stimulation of cholinergic system inhibits activation of nuclear factor-kappa B (NF-κB) [7] and induces suppressor of cytokine signal 3 expression [8], resulting in the attenuation of inflammatory responses. However, nicotine, a nicotinic acetylcholine receptor (AchR) agonist, was reported to induce endothelial dysfunction that is an initial step of atherosclerosis and to accelerate atherosclerosis in Apolipoprotein E-knockout (ApoE-KO) mice [9]. Therefore, it is not clear whether the activation of cholinergic system is atherogenic or atheroprotective.

Donepezil [diethyl(3,5-di-ter-butyl-4-hydroxybenzyl)phosphonate] is a long acting, reversible cholinesterase inhibitor and is known to improve memory and cognitive function in patients with Alzheimer's disease [10]. A recent study showed that treatment of patients with Alzheimer's disease with donepezil for 1 month reduces production of oncostatin-M, interleukin (IL)-6 and IL-1 in the peripheral blood mononuclear cells [11], suggesting a possible anti-inflammatory effect of donepezil. However, the mechanism remains to be determined.

Angiotensin (Ang) II plays critical roles in the progression of atherosclerosis, ventricular remodeling after myocardial infarction and heart failure [12]. One of the mechanisms by which AngII

* Corresponding author at: Department of Cardiovascular Medicine, Kyushu University Graduate School of Medical Sciences, 3-1-1 Maidashi, Higashiku, 812-8582 Fukuoka, Japan. Tel.: +81 92 642 5361; fax: +81 92 642 5374.
E-mail address: ichiki@cardiol.med.kyushu-u.ac.jp (T. Ichiki).

0021-9150/$ – see front matter © 2010 Elsevier Ireland Ltd. All rights reserved.
doi:10.1016/j.atherosclerosis.2010.07.027

accelerates atherogenesis is the induction of oxidative stress and inflammation [13]. AngII activates NADPH oxidase in the blood vessel resulting in the activation of redox-sensitive transcription factors such as nuclear factor (NF)-B and activating protein (AP)-1 [14], resulting in the production of inflammatory cytokines or chemokines such as TNF-α, IL-6, and monocyte chemoattractant protein (MCP)-1.

These previous studies prompted us to examine the effect of pharmacological stimulation of cholinergic system by donepezil on the progression of atherosclerosis in ApoE-KO mice. In the present study we showed that donepezil attenuated atherogenesis in ApoE-KO mice fed a high-fat diet (HFD) with or without AngII stimulation, possibly through anti-oxidative and anti-inflammatory effects.

2. Materials and methods

2.1. Materials

AngII was purchased from PEPTIDE Institute Inc. Physostigmine, Ach, lucigenin, β-nicotinamide adenine dinucleotide 2′-phosphate reduced hydrate (NADPH) were purchased from Sigma Chemical Co. Donepezil was purchased from Toronto Research Chemicals Inc. Antibodies against p47phox and NOX1 were purchased from Santa Cruz Biotechnology, Inc. Other chemical reagents were purchased from Wako Pure Chemicals, unless mentioned specifically.

2.2. Animal model of atherosclerosis

All procedures were approved by the committee on Ethics of Animal Experiment, Kyushu University Graduate School of Medical Sciences and conducted in accordance with the Guide for the Care and Use of Laboratory Animals published by the US National Institutes of Health.

C57BL/6J ApoE-KO mice were purchased from the Jackson Laboratory. Male ApoE-KO (10-week-old) mice were fed a HFD (35% calorie from fat, 1% cholesterol) and received infusion of AngII (490 ng/kg/day) through an osmotic minipump (Alzet) implanted in the peritoneal cavity for 4 weeks. Mice had an ad libitum access to both food and water. Four groups were compared: control, AngII + HFD, AngII + HFD and donepezil (estimated dose of ingestion: 5 mg/kg/day via drinking water), and AngII + HFD and physostigmine (2 mg/kg/day via second osmotic minipump). Blood pressure and heart rate were monitored using a computed tail-cuff system (UR-5000, UEDA, Ueda Co. Ltd.). The doses of cholinesterase inhibitors were chosen on the basis of previous studies that showed that donepezil [15] or physostigmine [16] at the doses mentioned above did not affect heart rate or blood pressure level in mice.

In another experiment, ApoE-KO mice (12-week-old) were fed a HFD only for 8 weeks without AngII. And the effect of donepezil was examined.

2.3. Histological and immunohistochemical analyses

At the end of experiments, mice were anesthetized with an intraperitoneal injection of pentobarbital. The circulatory system was perfused with PBS via the left ventricle. Then, the aortic arch and the thoracic aorta was opened longitudinally, stained with Oil Red O, and pinned out on a black wax surface. The percentage of the plaque area stained by Oil Red O to the total luminal surface area was determined. Serial sections of the aortic root were prepared and were stained with the antibodies against macrophage (F4/80; Serotec Inc.) and MCP-1 (Santa Cruz Biotechnology Inc.). All images were captured with a Nikon microscope equipped with a video camera and analyzed using Adobe Photoshop and Scion Image Software.

2.4. Tissue preparation

The thoracic and abdominal aorta were immediately frozen in liquid nitrogen for RNA isolation, Lucigenin assay, and Western blot analysis. For RNA isolation, thoracic aorta was additionally perfused with RNA Later (Ambion) to prevent RNA degradation. Frozen samples of thoracic aorta were crashed on dry ice and homogenized in ISOGEN (Nippon Gene) and total RNA was prepared in accordance with the manufacturer's instruction.

2.5. Real-time reverse transcription polymerase chain reaction analysis

Reverse transcription of RNA was performed with ReverTra Ace (TOYOBO). Quantitative real-time reverse transcription polymerase chain reaction (qRT-PCR) was performed using SYBR Green and the ABI PRISM 7500 Sequence Detection System (Applied Biosystems). The sequences of PCR primers used in this study are summarized in Supplemental Table 1. Primers for GAPDH were purchased from ABI, of which sequences are not disclosed.

2.6. Lucigenin-enhanced chemiluminescence assay

NADPH-dependent superoxide production was measured by lucigenin luminescence [17]. The aorta was perfused with ice cold PBS, immediately frozen in liquid nitrogen and the assay was performed on the same day. The frozen samples of abdominal aorta were crashed on dry ice and homogenized in modified Krebs buffer (99 mmol/L NaCl, 4.7 mmol/L KCl, 1.9 mmol/L $CaCl_2$, 1.2 mmol/L $MgSO_4$, 1.0 mmol/L K_2HPO_4, 25 mmol/L $NaHCO_3$, 20 mmol/L Na-HEPES, 11 mmol/L D-glucose). A luminescence assay was performed in a balanced salt solution (137 mmol/L NaCl, 2.7 mmol/L KCl, 4.3 mmol/L Na_2HpO_4, 1.5 mmol/L KH_2PO_4) buffer containing 5 μmol/L of lucigenin using a luminescence reader (Berthold Technology). The reaction was started by adding 100 μmol/L of β-NADPH as a substrate.

2.7. Oxidative fluorescent microphotography

Superoxide was detected in the layers of the vessel wall using fluorescent probe dihydroethidium (DHE; Molecular Probes) as described previously [18]. After perfusion with ice cold PBS, the ascending thoracic aorta was immediately frozen in OCT compound (Sakura Finetek) and stored at −80 °C until preparation for the cryosection. Cryosections (10 μm) were prepared in the next day and incubated for 30 min at 37 °C with 2 μmol/L DHE. Images were obtained on a confocal microscope (excitation filter at 488 nm; emission filter at 550 nm).

2.8. Western blot analysis

The aorta was homogenized in modified Krebs buffer. Protein concentrations were determined with the bicinchoninic acid protein assay kit (Pierce Chemical Co). The homogenates were heated in a sample buffer at 95 °C for 3 min, electrophoresed on 12% SDS-polyacrylamide gel, and transferred to polyvinylidene difluoride membrane (Immobilon-P, Millipore). Western blot analysis of p47phox, NOX1 and α-tubulin was performed by a conventional method and detected by ECL chemiluminescence (Amersham Pharmacia Biotech) according to the manufacturer's instructions. Membranes were scanned using LAS-4000mini bioimage analyzer (Fujifilm).

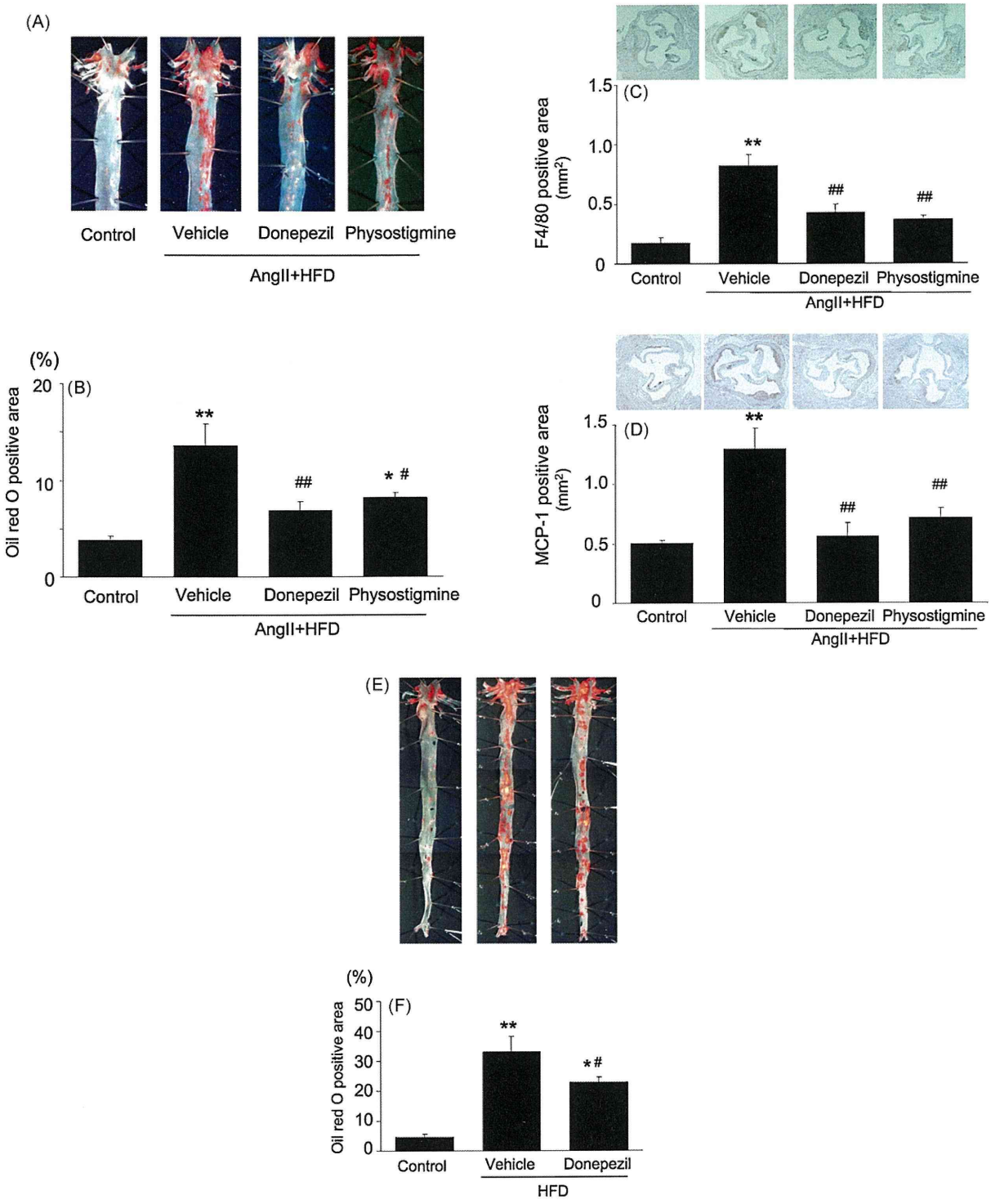

Fig. 1. Cholinesterase inhibitors attenuated atherogenesis in ApoE-KO mice. The effects of donepezil and physostigmine were examined in ApoE-KO mice fed a HFD and received AngII-infusion for 4 weeks (A–D). $n = 6$–8 (A) Oil Red O staining of the en face aorta is shown. (B) Bar graph indicates the percentage of Oil Red O-positive area in the aorta. (C) Immunohistochemical staining for macrophage by F4/80 antibody in the aortic cusp. Bar graph indicates F4/80-positive area. (D) Immunohistochemical staining for MCP-1 in the aortic cusp. Bar graph indicates MCP-1-positive area. Data are expressed as mean ± S.E.M. $^{*}P < 0.05$, $^{**}P < 0.01$ vs control, $^{\#}P < 0.05$, $^{\#\#}P < 0.05$ vs vehicle. The effect of donepezil was examined in ApoE-KO mice fed a HFD for 8 weeks (E and F). (E) Oil Red O staining of the en face aorta is shown. (F) Bar graph indicates the percentage of Oil Red O-positive area in the aorta. Data are expressed as mean ± S.E.M. $^{**}P < 0.01$ vs control, $^{\#}P < 0.05$ vs vehicle. Control $n = 5$, HFD or HFD + donepezil $n = 8$.

Table 1
HR, BP BW and total cholesterol levels in AngII + HFD groups.

	HR (bpm)	BP (mm Hg)	BW (g)	TC (mg/dl)
Control	610 ± 20	104 ± 2	28.8 ± 0.6	407 ± 21
AII + HFD	648 ± 17	124 ± 4**	27.2 ± 0.4	1981 ± 165**
AII + HFD + donepezil	618 ± 22	115 ± 4*	27.7 ± 1.0	1896 ± 63**
AII + HFD + physostigmine	657 ± 8	124 ± 3**	27.9 ± 0.7	2250 ± 70**

HR: heart rate, BP: blood pressure, BW: body weight, TC: total cholesterol.
* $P < 0.05$ vs control.
** $P < 0.01$ vs control.

2.9. Statistical analysis

Statistical analysis was performed with one-way ANOVA and Fisher's test, if appropriate. Data are shown as mean ± S.E.M. $P < 0.05$ was considered to be statistically significant.

3. Results

3.1. Cholinesterase inhibitors attenuated progression of atherosclerosis

To examine whether donepezil has anti-inflammatory and anti-atherosclerotic effects, we used HFD-fed ApoE-KO mice with AngII that accelerates vascular inflammation and thereby atherogenesis [13]. A combination treatment with AngII and HFD significantly increased blood pressure compared with control group. However, no significant differences in the heart rate, blood pressure and serum total cholesterol level were observed between AngII and HFD groups (Table 1). Body weight was slightly decreased in mice that received AngII and HFD compared with the control group. Oil Red O-positive area of en face aorta was reduced in mice treated with donepezil (Fig. 1A and B). Physostigmine, another cholinesterase inhibitor structurally unrelated to donepezil, also reduced Oil Red O-positive area, suggesting that inhibition of cholinesterase and a resultant increase in Ach availability are responsible for the attenuation of atherogenesis (Fig. 1A and B). Infiltration of macrophage (F4/80 antibody-positive cells) into the aortic root was also reduced in mice treated with donepezil or physostigmine (Fig. 1C). These cells expressed MCP-1 (Fig. 1D) and MCP-1-positive area was diminished by treatment with either donepezil or physostigmine, suggesting that cholinesterase inhibitors may attenuate atherogenesis through suppression of MCP-1 expression and macrophage recruitment.

We also examined the effect of donepezil on ApoE-KO mice fed a HFD for 8 weeks (from 12- to 20-week-old) without AngII-infusion. The Oil Red O-positive area was significantly suppressed by treatment with donepezil (Fig. 1E and 1F) without effects on hemodynamics and cholesterol level (Table 2).

3.2. Donepezil attenuated vascular reactive oxygen species (ROS) production and NADPH oxidase activity

ROS play an important role in atherogenesis. We, therefore, examined the effect of donepezil on ROS production. DHE staining showed that vascular ROS production was increased in ApoE-KO mice treated with AngII and HFD and that donepezil reduced the ROS production in the media (Fig. 2A). Lucigenin assay also showed that donepezil significantly reduced NADPH oxidase activity that is increased in AngII- and HFD-treated ApoE-KO mice (Fig. 2B). However, we did not see any effect of donepezil on the serum level of thiobarbituric acid reactive substance (data not shown), suggesting that donepezil might locally suppress oxidative stress in the aorta.

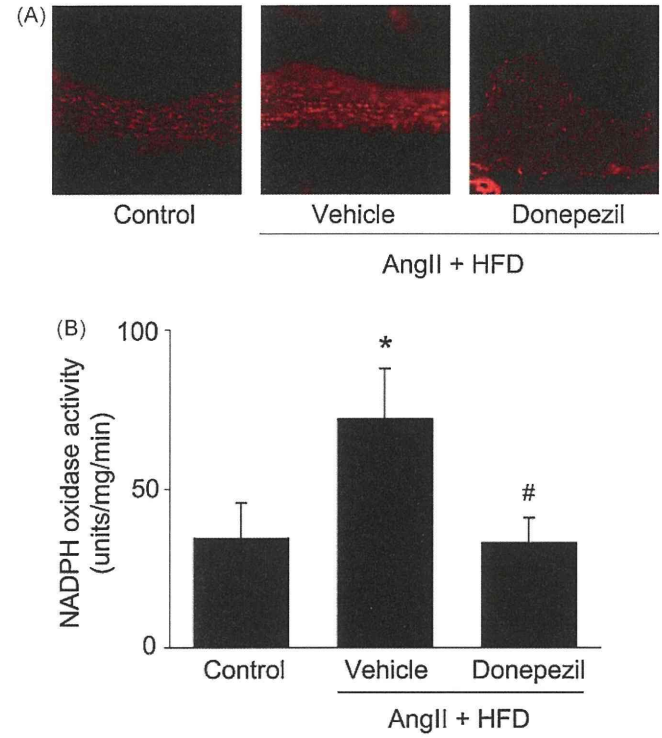

Fig. 2. The effect of donepezil on the oxidative stress in the aorta of ApoE-KO mice. (A) DHE staining revealed an increase in superoxide production in the aorta of AngII- and HFD-treated ApoE-KO mice. Donepezil reduced the extent of DHE staining. The same results were obtained in other 5 independent experiments. (B) Lucigenin assay showed that NADPH oxidase activity was increased by treatment with AngII and HFD in the aorta of ApoE-KO mice. Donepezil reduced the NADPH oxidase activity. Data are expressed as mean ± S.E.M. *$P < 0.05$ vs control, #$P < 0.05$ vs vehicle. $n = 6–8$.

Table 2
HR, BP BW and total cholesterol levels in HFD groups.

	HR (bpm)	BP (mm Hg)	BW (g)	TC (mg/dl)
Control	537 ± 13	99 ± 1	30.8 ± 0.6	555 ± 28
HFD	579 ± 15	97 ± 5	27.5 ± 0.7*	2173 ± 200**
HFD + donepezil	539 ± 19	100 ± 4	28.6 ± 1.2	2001 ± 96**

HR: heart rate, BP: blood pressure, BW: body weight, TC: total cholesterol.
* $P < 0.05$ vs control.
** $P < 0.01$ vs control.

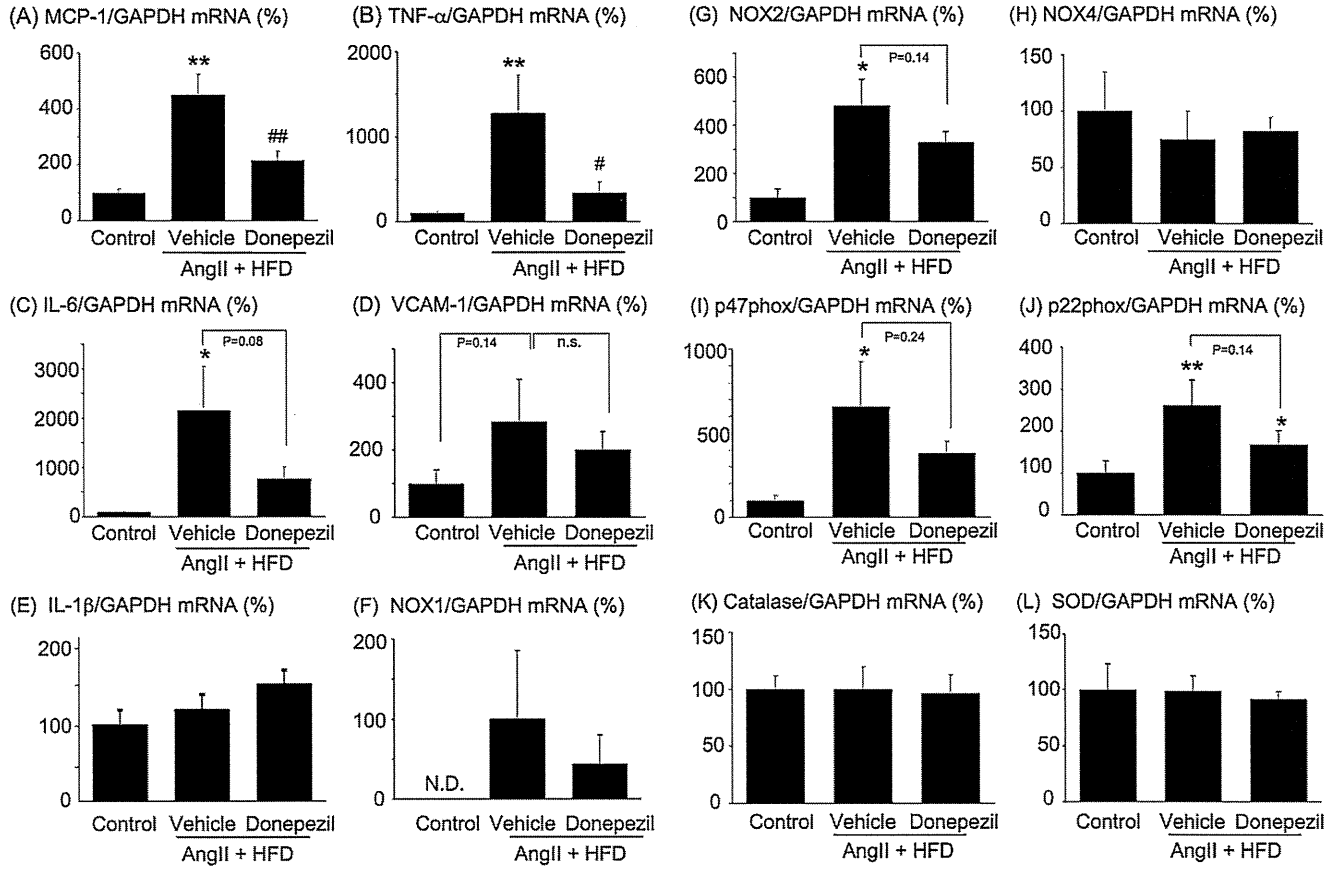

Fig. 3. Quantitative RT-PCR analyses for the mRNA expression in the aorta. mRNA expression of the aorta from control, AngII- and HFD- and AngII-, HFD- and donepezil-treated ApoE-KO mice was quantified with real-time RT-PCR. The primer sequences used were indicated in Supplemental Table 1. Data are expressed as mean ± S.E.M. $^{*}P < 0.05$, $^{**}P < 0.01$ vs control, $^{\#}P < 0.05$, $^{\#\#}P < 0.01$ vs vehicle. $n = 7–8$. ND; not detected.

3.3. Donepezil attenuated MCP-1 and TNF-α mRNA expression

To gain insights into the molecular mechanism of anti-atherogenic effect of donepezil, mRNA expression of the aorta was examined by RT-PCR (Fig. 3). The combination treatment with AngII and HFD significantly increased MCP-1 and TNF-α mRNA expression in the aorta of ApoE-KO mice. Donepezil significantly attenuated both MCP-1 and TNF-α mRNA expression.

NOX1 is a major NADPH oxidase subunit expressed in VSMC [19]. Expression of NOX1 was slightly increased by AngII and a HFD, which was downregulated by donepezil. However, expression level of NOX1 is very low and the difference was not statistically significant.

Expression of other NADPH oxidase subunits (NOX2, p22phox, p47phox) was significantly increased in AngII and HFD group and donepezil attenuated the mRNA expression of these molecules. However, the reduction was not statistically significant. mRNA expression of NOX4, one of the NADPH oxidase subunit, superoxide dismutase, and catalase was not affected by the combination treatment with AngII and a HFD.

3.4. Donepezil inhibited p47phox and NOX1 protein level in the aorta

We examined protein expression of p47phox and NOX1 in the aorta. Western blot analysis revealed that expression level of p47phox was increased in ApoE-KO mice treated with HFD and AngII and the induction was significantly suppressed by donepezil (Fig. 4). The protein level of NOX1 was not affected among the three groups.

4. Discussion

We showed in the present study that donepezil and physostigmine attenuated progression of AngII accelerated atherosclerosis in ApoE-KO mice fed a HFD. The anti-atherogenic effect of donepezil was also observed in ApoE-KO mice fed a HFD without AngII-infusion. Donepezil attenuated NADPH oxidase activity and ROS production as well as cytokine expression in the aorta. These results suggest that cholinesterase inhibitor may be a novel strategy for the treatment of atherosclerotic cardiovascular diseases.

We chose ApoE-KO mice treated with HFD and AngII as an atherosclerotic model because AngII is known to induce inflammation and our hypothesis is that donepezil has an anti-inflammatory effect. It is of note that donepezil was more effective in HFD and AngII-infusion group than HFD group. Therefore, donepezil may be more effective against AngII-induced atherogenesis.

Custodis et al. showed that heart rate reduction by ivabradine, an inhibitor of I_f current in the sinoatrial node, attenuated atherogenesis in ApoE-KO mice [20]. In the present study, neither donepezil nor physostigmine significantly decreased heart rate, excluding the possible suppressive effect of bradycardia on atherogenesis. However, the reason why heart rate was not decreased by these cholinesterase inhibitors in our mice is not clear.

A recent meta-analysis by Singh et al. revealed that inhalation of anticholinergics is associated with a significantly increased risk of myocardial infarction and cardiovascular death but not with a risk of stroke in patients with chronic obstructive pulmonary disease (COPD) [21]. The results of the meta-analysis may support the idea that cholinergic system is atheroprotective. However, a very recent

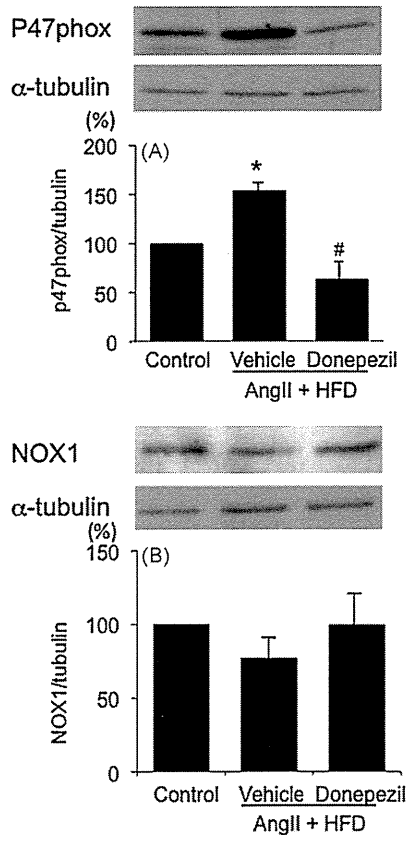

Fig. 4. Expression of p47phox and NOX1 protein in the aorta. Expression of p47phox and NOX1 protein was examined by Western blot analysis in the aorta of control, AngII- and HFD-, and AngII-, HFD- and donepezil-treated ApoE-KO mice. The blot was scanned and the band density was quantified. Data are expressed as mean ± S.E.M. $^{*}P < 0.05$ vs control, $^{\#}P < 0.05$ vs HFD and AngII group. $n = 4$.

double-blind trial that examined the effect of tiotropium, one of the anticholinergics, in patients with COPD showed opposite results [22]. Treatment with tiotropium showed an insignificant decrease in the number of death in patients with COPD and significantly decreased the incidence of myocardial infarction compared with placebo. Therefore, the issue regarding the effect of anticholinergics treatment on cardiovascular events, in particular myocardial infarction, is still controversial.

Vascular oxidative stress accelerates atherosclerosis [23]. AngII induces ROS production via activation of NADPH oxidase. Subunits of NADPH oxidase such as p47phox, p22phox, and NOX play critical role in AngII induced ROS production because knockdown of these subunit inhibited ROS production by AngII and less vascular lesion was induced in mice lacking these subunit [19]. The reduction of mRNA expression of each NADPH oxidase subunits (p47phox, p22phox and NOX1) in donepezil-treated mice was not statistically significant. However, the expression of p47phox at the protein level was significantly reduced by donepezil. Although the mechanism for the difference between mRNA and protein level of p47phox is not clear, suppression of p47phox may explain the anti-oxidative effect of donepezil.

Donepezil suppressed aortic MCP-1 expression in ApoE-KO mice received HFD and AngII-infusion. MCP-1 is well known to enhance atherogenesis. However, MCP-1 deficiency did not affect atherosclerotic lesion size in LDL receptor knockout mice fed a normal chow but decreased lesion size those fed a western diet [24]. The lack of the effect of MCP-1 deficiency is explained by upregulation of MCP-5, which is highly homologous to MCP-1. This study suggests that single inhibition of MCP-1 is not sufficient to suppress atherogenesis due to activation of alternative pathways. In this regard, simultaneous suppression of TNF-α by donepezil might synergistically attenuate atherogenesis in ApoE-KO mice. A recent study showed that expression of hepatic MCP-1 mRNA was correlated with the degree of liver steatosis in LDL receptor knockout mice fed a HFD [25]. Therefore, it is interesting to address in the future whether donepezil ameliorates liver steatosis in ApoE-KO mice treated with a HFD and AngII-infusion.

Acetylcholine, a major neurotransmitter of vagus nerve, is known to activate endothelial nitric oxide (NO) synthase and dilate blood vessel [26]. However, acetylcholine is rapidly degraded by cholinesterase in a few seconds. Therefore, it may be possible that donepezil and physostigmine inhibition of cholinesterase increases the availability of acetylcholine and increases NO production. However, we could not see upregulation or phosphorylation of eNOS in the aorta of ApoE-KO mice treated with donepezil (data not shown). These data suggest that an increase in NO level may not be the major mechanism for the anti-atherosclerotic effect of donepezil.

At this point, the source of acetylcholine is not clear. Amenta et al. showed that cholinergic innervation of the aorta [27]. A nerve plexus in the adventitial layer has been identified in the mouse, suggesting that acetylcholine is derived from the nerve ending of the vagus. In contrast, recent studies suggest that macrophages and endothelial cells express choline acetyltransferase that produces acetylcholine from choline and acetyl-CoA [28]. Therefore, further study is needed to determine whether acetylcholine is derived from vagus nerve ending or locally produced from macrophages or endothelial cells.

The limitation of the present study is that we do not have a direct evidence that donepezil inhibited atherogenesis through an inhibition of cholinesterase. Because the dose of donepezil used in this study is very high, we could not exclude the possibility of a direct or non-specific anti-atherogenic effect of donepezil. However, physostigmine, another cholinesterase inhibitor structurally different from donepezil also suppressed atherogenesis in the same model, indicating that the anti-atherogenic effect is mediated by inhibition of cholinesterase but not by a direct or non-specific effect of the drug. Further study is needed to confirm this point.

Another limitation of the current study is that we used very high dose of donepezil compared with the dose clinically used for the treatment of Alzheimer's disease. Therefore, we must be cautious about extrapolating our results to human atherosclerosis. However, 5 mg/kg/day of donepezil is widely used to examine the effect on dementia in a rodent model [29] despite the clinical dose is 5–10 mg/day for Alzheimer's disease. Thus, differential susceptibility to the drug between human and mice, and a very short period for the development of the lesions in animal models may be the reason for the requirement for high doses to be effective.

In summary, we showed in the present study that treatment with donepezil attenuated atherogenesis in ApoE-KO mice possible through anti-oxidative and anti-inflammatory effects. Although we should be cautious in extrapolating current results to other atherosclerotic model or human atherosclerosis [30], cholinesterase inhibitors may be a novel strategy for the treatment of atherosclerotic cardiovascular diseases.

Acknowledgements

This study was supported in part by Grants-in-aid for Scientific Research from the Ministry of Education, Culture, Sports, Science and Technology of Japan (19590867), AstraZeneca Research grant 2007 (London, UK), Mitsubishi Pharma Research Foundation (Osaka, Japan), Astellas Foundation for Research on Metabolic Disorders (Tokyo, Japan) and Suzuken Memorial Foundation (Nagoya, Japan).

Appendix A. Supplementary data

Supplementary data associated with this article can be found, in the online version, at doi:10.1016/j.atherosclerosis.2010.07.027.

References

[1] Schwartz PJ, La Rovere MT. ATRAMI: a mark in the quest for the prognostic value of autonomic markers. Autonomic Tone and Reflexes After Myocardial Infarction. Eur Heart J 1998;19:1593–5.
[2] The Cardiac Insufficiency Bisoprolol Study II (CIBIS-II): a randomised trial. Lancet 1999;353:9–13.
[3] Li M, Zheng C, Sato T, et al. Vagal nerve stimulation markedly improves long-term survival after chronic heart failure in rats. Circulation 2004;109:120–4.
[4] Tsutsumi T, Ide T, Yamato M, et al. Modulation of the myocardial redox state by vagal nerve stimulation after experimental myocardial infarction. Cardiovasc Res 2008;77:713–21.
[5] Borovikova LV, Ivanova S, Zhang M, et al. Vagus nerve stimulation attenuates the systemic inflammatory response to endotoxin. Nature 2000;405:458–62.
[6] Wang H, Yu M, Ochani M, et al. Nicotinic acetylcholine receptor alpha7 subunit is an essential regulator of inflammation. Nature 2003;421:384–8.
[7] Wang H, Liao H, Ochani M, et al. Cholinergic agonists inhibit HMGB1 release and improve survival in experimental sepsis. Nat Med 2004;10:1216–21.
[8] de Jonge WJ, van der Zanden EP, The FO, et al. Stimulation of the vagus nerve attenuates macrophage activation by activating the Jak2-STAT3 signaling pathway. Nat Immunol 2005;6:844–51.
[9] Heeschen C, Jang JJ, Weis M, et al. Nicotine stimulates angiogenesis and promotes tumor growth and atherosclerosis. Nat Med 2001;7:833–9.
[10] Hansen RA, Gartlehner G, Webb AP, et al. Efficacy and safety of donepezil, galantamine, and rivastigmine for the treatment of Alzheimer's disease: a systematic review and meta-analysis. Clin Interv Aging 2008;3:211–25.
[11] Reale M, Iarlori C, Gambi F, et al. Acetylcholinesterase inhibitors effects on oncostatin-M, interleukin-1 beta and interleukin-6 release from lymphocytes of Alzheimer's disease patients. Exp Gerontol 2005;40:165–71.
[12] Dzau V. The cardiovascular continuum and renin–angiotensin–aldosterone system blockade. J Hypertens Suppl 2005;23:S9–17.
[13] Ni W, Kitamoto S, Ishibashi M, et al. Monocyte chemoattractant protein-1 is an essential inflammatory mediator in angiotensin II-induced progression of established atherosclerosis in hypercholesterolemic mice. Arterioscler Thromb Vasc Biol 2004;24:534–9.
[14] Garrido AM, Griendling KK. NADPH oxidases and angiotensin II receptor signaling. Mol Cell Endocrinol 2009;302:148–58.
[15] Handa T, Katare RG, Kakinuma Y, et al. Anti-Alzheimer's drug, donepezil, markedly improves long-term survival after chronic heart failure in mice. J Card Fail 2009;15:805–11.
[16] Bhat RV, Turner SL, Marks MJ, Collins AC. Selective changes in sensitivity to cholinergic agonists and receptor changes elicited by continuous physostigmine infusion. J Pharmacol Exp Ther 1990;255:187–96.
[17] Miller Jr FJ, Griendling KK. Functional evaluation of nonphagocytic NAD(P)H oxidases. Methods Enzymol 2002;353:220–33.
[18] Chun HJ, Ali ZA, Kojima Y, et al. Apelin signaling antagonizes Ang II effects in mouse models of atherosclerosis. J Clin Invest 2008;18:3343–54.
[19] Brandes RP, Schroder K. Composition and functions of vascular nicotinamide adenine dinucleotide phosphate oxidases. Trends Cardiovasc Med 2008;18:15–9.
[20] Custodis F, Baumhakel M, Schlimmer N, et al. Heart rate reduction by ivabradine reduces oxidative stress, improves endothelial function, and prevents atherosclerosis in apolipoprotein E-deficient mice. Circulation 2008;117:2377–87.
[21] Singh S, Loke YK, Furberg CD. Inhaled anticholinergics and risk of major adverse cardiovascular events in patients with chronic obstructive pulmonary disease: a systematic review and meta-analysis. JAMA 2008;300:1439–50.
[22] Tashkin DP, Celli B, Senn S, et al. 4-Year trial of tiotropium in chronic obstructive pulmonary disease. N Engl J Med 2008;359:1543–54.
[23] Cai H, Harrison DG. Endothelial dysfunction in cardiovascular diseases: the role of oxidant stress. Circ Res 2000;87:840–4.
[24] Rull A, Beltrán-Debón R, Aragonès G, et al. Expression of cytokine genes in the aorta is altered by the deficiency in MCP-1: effect of a high-fat, high-cholesterol diet. Cytokine 2010;50:121–8.
[25] Rull A, Rodríguez F, Aragonès G, et al. Hepatic monocyte chemoattractant protein-1 is upregulated by dietary cholesterol and contributes to liver steatosis. Cytokine 2009;48:273–9.
[26] Pepine CJ. The impact of nitric oxide in cardiovascular medicine: untapped potential utility. Am J Med 2009;122:S10–5.
[27] Amenta F, Cavallotti C, Ferrante F, Zomparelli M. The cholinergic innervation of the aorta. Acta Histochem 1980;66:197–203.
[28] Wessler I, Kirkpatrick CJ, Racke K. The cholinergic 'pitfall': acetylcholine, a universal cell molecule in biological systems, including humans. Clin Exp Pharmacol Physiol 1999;26:198–205.
[29] Saxena G, Singh SP, Agrawal R, Nath C. Effect of donepezil and tacrine on oxidative stress in intracerebral streptozotocin-induced model of dementia in mice. Eur J Pharmacol 2008;581:283–9.
[30] Joven J, Rull A, Ferré N, et al. The results in rodent models of atherosclerosis are not interchangeable: the influence of diet and strain. Atherosclerosis 2007;195(2):e85–92.

Blockade of mineralocorticoid receptors improves salt-induced left-ventricular systolic dysfunction through attenuation of enhanced sympathetic drive in mice with pressure overload

Koji Ito, Yoshitaka Hirooka and Kenji Sunagawa

Objectives In a pressure overload model, sympathetic activity is augmented in response to salt intake. Mineralocorticoid receptors and epithelial Na channels (ENaCs) are thought to contribute to Na-processing, but the underlying mechanism is unknown. Here, we investigated the contribution of the brain mineralocorticoid receptor–ENaC pathway to salt-induced sympathetic activation in a pressure overload model.

Methods and results Aortic banding was performed to produce a mouse pressure overload model. Four weeks after aortic banding (AB-4), left-ventricular (LV) wall thickness was increased without a change in percentage fractional shortening (%FS). Sympathetic activity increased in response to a 5-day high-salt diet in AB-4, but not in Sham-4. Brain mineralocorticoid receptor, αENaC, and angiotensin II type 1 receptor (AT1R) expression levels were greater in AB-4 than in Sham-4. The increase in sympathetic activity and in the expression of these proteins was blocked by intracerebroventricular (ICV) infusion of eplerenone, a mineralocorticoid receptor blocker. In another protocol, AB-4 mice were fed a high-salt diet (AB-H) for 4 additional weeks. At 4 weeks, %FS was decreased and sympathetic activity was increased in AB-H compared with Sham. Expression of mineralocorticoid receptors and AT1R in the brain was higher in AB-H than in Sham. ICV infusion of eplerenone in AB-H attenuated salt-induced sympathoexcitation and the decreased %FS. ICV infusion of eplerenone also decreased brain AT1R expression.

Conclusions These findings indicate that activation of brain αENaC and AT1R through mineralocorticoid receptors contributes to the acquisition of Na sensitivity to induce sympathoexcitation. Therefore, high salt intake accelerates sympathetic activation and LV systolic dysfunction in a pressure overload model. *J Hypertens* 28:1449–1458 © 2010 Wolters Kluwer Health | Lippincott Williams & Wilkins.

Journal of Hypertension 2010, 28:1449–1458

Keywords: brain, heart failure, pressure overload, salt, sympathetic nervous system

Abbreviations: %FS, percent fractional shortening; AB-4, AB mice 4 weeks postoperative; AB-H, AB mice fed a high salt diet; AB-R, AB mice fed a regular salt diet; AT1R, angiotensin II type 1 receptor; CSF, cerebrospinal fluid; ENaCs, epithelial Na channels; GAPDH, glyceraldehyde 3-phosphate dehydrogenase; ICV, intracerebroventricular; IgG, immunoglobulin; LV, left ventricle; LVDD, LV end-diastolic diameter; LVSD, LV end-systolic diameter; LVWT, LV wall thickness; Sham, sham-operated mice; Sham-4, Sham mice 4 weeks postoperative; Sham-H, Sham mice fed a high salt diet; Sham-R, Sham mice fed a regular salt diet; U-NE, 24-h urinary norepinephrine

Department of Cardiovascular Medicine, Kyushu University Graduate School of Medical Sciences, Fukuoka, Japan

Correspondence to Yoshitaka Hirooka, MD, PhD, FAHA, Department of Cardiovascular Medicine, Kyushu University Graduate School of Medical Sciences, 3-1-1, Higashi-ku, Fukuoka 812-8582, Japan
Tel: +81 92 642-5360; fax: +81 92 642 5374;
e-mail: hyoshi@cardiol.med.kyushu-u.ac.jp

Received 8 September 2009 **Revised** 22 December 2009
Accepted 15 February 2010

Introduction

High salt intake induces hypertension in a salt-sensitive hypertensive animal model via sympathetic nerve activation [1,2]. The central nervous system plays an important role in salt-induced hypertension. An increase in Na in the cerebrospinal fluid (CSF) is an important step in salt-induced hypertension. High salt intake increases CSF Na only in salt-sensitive hypertensive rats, however, and not in salt-resistant normotensive rats [3]. Intracerebroventricular (ICV) infusion of high-Na containing CSF causes hypertension in both salt-sensitive hypertensive rats and salt-resistant normotensive rats via brain angiotensin type 1 receptor (AT1R) activation [4]. Enhanced Na uptake from the plasma to the CSF might therefore be an important step in the initiation of salt-induced hypertension in salt-sensitive hypertensive rats. Epithelial Na channels (ENaCs) on the blood side of the choroidal epithelium contribute to Na transport in the CSF [5,6]. In addition, ENaCs are activated through the activation of mineralocorticoid receptors [7,8]. Thus, the mineralocorticoid receptor–ENaC pathway might be involved in the enhanced Na uptake into the CSF in the salt-sensitive hypertensive model.

We recently reported that mice with pressure overload become sensitive to physiologic brain levels of Na, thereby acquiring a lower threshold for sympathetic activation [9]. Whether the brain mineralocorticoid receptor–ENaC pathway is involved in the salt-sensitive sympathetic activation in mice with pressure overload, however, is not clear. Therefore, the aim of the present study was to examine the expression levels of brain mineralocorticoid receptors and ENaCs in mice with pressure overload, and to determine whether mineralocorticoid receptor

0263-6352 © 2010 Wolters Kluwer Health | Lippincott Williams & Wilkins DOI:10.1097/HJH.0b013e328338bb37

Fig. 1

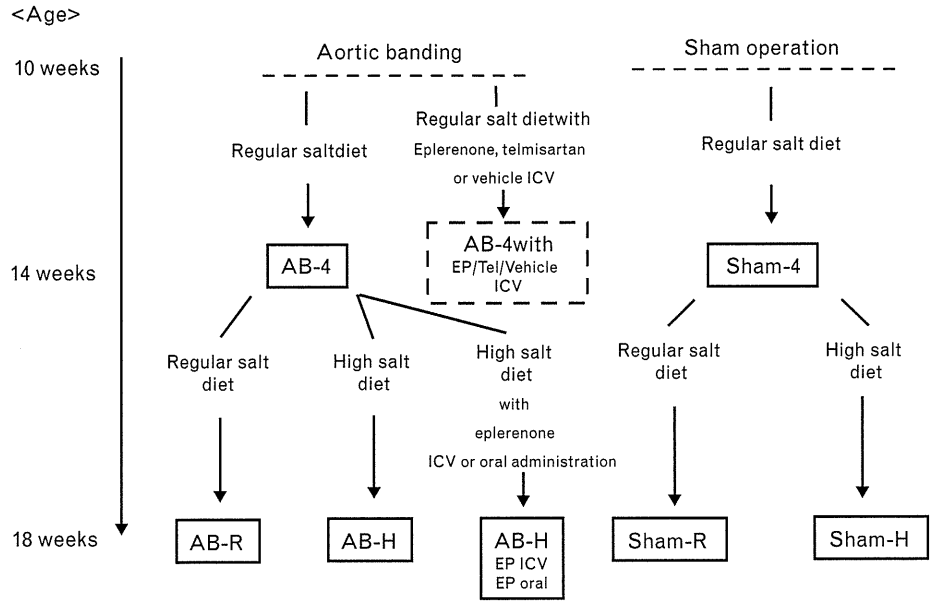

Experimental protocol and time-line. W indicates weeks; ICV, intracerebroventricular.

antagonism attenuates salt-induced sympathetic activation and improves left-ventricular (LV) systolic function in mice with pressure overload. Toward this aim, we investigated the expression of brain mineralocorticoid receptor and ENaCs in mice with pressure overload; the sympathetic activity in response to a 5-day high-salt diet in mice with pressure overload to confirm the acquisition of Na sensitivity; the effects of ICV infusion or oral administration of eplerenone, a selective mineralocorticoid receptor blocker [10,11], concomitant with high-salt loading on sympathetic activity and LV systolic function in mice with pressure overload.

Methods

Animals

The study was reviewed and approved by the Committee on Ethics of Animal Experiments, Kyushu University Graduate School of Medical Sciences, and conducted according to the Guidelines for Animal Experiments of Kyushu University. Male Institute of Cancer Research (ICR) mice (10 weeks old; SLC, Fukuoka, Japan) were used.

Mouse pressure overload model preparation

The suprarenal abdominal aorta [9,12] was banded in mice (AB mice) under sodium pentobarbital (25–40 mg/kg i.p.) anesthesia. The abdominal aorta was constricted at the suprarenal level with 5-0 silk sutures guided by a blunted 27-gauge needle, which was withdrawn as quickly as possible. Sham-operated (Sham) mice served as controls. Four weeks later, mice (AB-4 mice or Sham-4 mice) were each divided randomly into two groups: mice fed a high-salt (8% NaCl) diet for 4 weeks (AB-H mice and Sham-H mice) and mice fed a regular-salt (0.3% NaCl) diet for 4 weeks (AB-R mice and Sham-R mice; Fig. 1).

Evaluation of left-ventricular systolic function

Left-ventricular systolic function was evaluated by echocardiography [9,13,14]. Serial M-mode echocardiography was performed on mice under light sodium pentobarbital anesthesia with spontaneous respiration. We used an echocardiography system (SSD5000; Aloka, Tokyo, Japan) with a dynamically focused 7.5-MHz linear array transducer. M-mode tracings were recorded from the short-axis view at the level of the papillary muscle. Left ventricle end-diastolic diameter (LVDD), LV end-systolic diameter (LVSD), and LV wall thickness (LVWT) were measured. LVWT was calculated as the mean thickness of the interventricular septum and the posterior LV wall. Percentage fractional shortening (%FS) was calculated as follows: $\%FS = (LVDD - LVSD)/LVDD \times 100$.

Evaluation of sympathetic activity

Sympathetic activity was evaluated by measuring 24-h urinary norepinephrine (U-NE) excretion using high-performance liquid chromatography [9,13,14].

Confirmation of acquired Na sensitivity in AB-4 mice

Sympathetic activity in response to a 5-day high-salt diet was evaluated as follows: both AB-4 mice and Sham-4

mice were fed a high-salt diet (8%) or a regular-salt diet for 5 days, and then U-NE was measured. Sympathetic activity in response to the high salt intake was evaluated in each group. In addition, ICV infusion of high-Na (0.2 mol/l) or regular-Na (0.145 mol/l) CSF (infusion rate: 0.25 μl/h for 5 days) was performed using an osmotic minipump, as follows. Under sodium pentobarbital anesthesia (25–40 mg/kg i.p.), mice were placed in a stereotaxic frame. The skin overlying the midline of the skull was incised, and a small hole was made with a dental drill at the following coordinates: 0.3 mm posterior and 1 mm lateral relative to bregma. The infusion cannula from an Alzet brain infusion kit 3 (DURECT Corporation, CA) connected to an osmotic minipump (Alzet model 1004; DURECT) was lowered 3 mm from the skull surface and fixed to the skull surface with tissue adhesive. The osmotic minipump was inserted subcutaneously in the back [9].

Measurement of organ weight

After completion of the experiments, the mice were killed with an overdose of sodium pentobarbital, and the heart and lungs were removed and weighed.

Measurement of blood pressure and heart rate

Under sodium pentobarbital anesthesia (25–40 mg/kg i.p.), mice were intubated using a 20-gauge soft catheter and ventilated with a tidal volume of 1.0–1.5 ml at 120 cycles/min with the fraction of inspired oxygen equal to 0.21 [9,13,14]. A catheter was then inserted into the right carotid artery to measure blood pressure and heart rate.

Treatment with eplerenone, a mineralocorticoid receptor blocker

To evaluate the effects of brain mineralocorticoid receptor antagonism on sympathetic activity in response to the high-salt diet in AB-4 mice, ICV infusion of the specific mineralocorticoid receptor blocker eplerenone [10,11] (0.3 mg/ml in CSF, infusion rate at 0.11 μl/h, kindly provided by Pfizer Pharmaceutical Company Inc., New York, New York, USA) was started concomitant with the aortic banding procedure and continued for 4 weeks. ICV infusion was performed as described above.

In another protocol, to evaluate the effects of brain mineralocorticoid receptor antagonism on salt-induced sympathetic activation and LV systolic dysfunction, eplerenone was administered by ICV infusion (0.3 mg/ml in CSF, infusion rate at 0.11 μl/h) or oral administration (100 mg/kg per day) for 4 weeks, concomitant with high-salt loading (AB-H mice). U-NE excretion, organ weight, blood pressure, and heart rate were measured, and echocardiography was performed as described above.

Evaluation of brain mineralocorticoid receptor, epithelial Na channels, and AT1R expression

The animals were killed with an overdose of sodium pentobarbital, and the circumventricular tissues including the hypothalamus were obtained. The tissues were homogenized in a lysing buffer containing 40 mmol/l HEPES [4-(2-hydroxyethyl)-1-piperazineethanesulfonic acid], 1% Triton X-100, 10% glycerol, 1 mmol/l sodium orthovanadate, and 1 mmol/l phenylmethylsulfonyl fluoride. Protein concentration was determined using a bicinchoninic acid protein assay kit (Pierce Chemical Co., Rockford, Illinois, USA). A 15-μg aliquot of protein from each sample was separated on a polyacrylamide gel with 10% sodium dodecyl sulfate. The proteins were subsequently transferred onto polyvinylidene difluoride membranes (Immobilon-P membranes; Millipore, Billerica, Massachusetts, USA). Membranes were incubated with rabbit immunoglobulin G (IgG) polyclonal antibody to mineralocorticoid receptors (1 : 1000; Santa Cruz Biotechnology, Santa Cruz, California, USA), with goat IgG polyclonal antibody to αENaC, rabbit polyclonal antibody to βENaC, rabbit polyclonal antibody to γENaC (1 : 1000, Santa Cruz Biotechnology), or with rabbit IgG monoclonal antibody to AT1R (1 : 1000, Santa Cruz Biotechnology). Membranes were then incubated with horseradish peroxidase-conjugated horse antirabbit or antigoat IgG antibody (1 : 10 000). Glyceraldehyde 3-phosphate dehydrogenase (GAPDH) was used as an internal control for the brain tissues. Immunoreactivity was detected by enhanced chemiluminescence autoradiography (ECL Western blotting detection kit; Amersham Pharmacia Biotech, Uppsala, Sweden), and the film was analyzed using the public domain software NIH Image (developed at the US National Institutes of Health and available on the Internet at http://rsb.info.nih.gov/nih-image/).

Evaluation of effects of eplerenone on brain epithelial Na channels and AT1R expression

To evaluate the effects of brain mineralocorticoid receptor antagonism on AT1R and ENaCs, we performed western blot analysis for AT1R, αENaC, and γENaC in the circumventricular tissues including the hypothalamus of AB-4 mice (AT1R and αENaC) or AB-H mice(AT1R and γENaC) with or without ICV infusion of eplerenone. ICV infusion of eplerenone and western blot analysis were performed as described above.

Evaluation of the effects of telmisartan, an AT1R blocker, on brain mineralocorticoid receptor and αENaC expression

To evaluate the effects of brain AT1R blockade on brain mineralocorticoid receptor and αENaC expression in AB-4 mice, we performed western blot analysis of mineralocorticoid receptor and αENaC in the circumventricular tissues, including the hypothalamus, of AB-4 mice with or without ICV infusion of telmisartan. ICV infusion of the AT1R blocker telmisartan [4 mmol/l in dimethyl sulfoxide (DMSO, Sigma Chemical Co) infusion rate at 0.11 μl/h for 28 days] [9] and western blot analysis were performed as described above.